

## Analysis of polished polycrystalline diamond using dual beam focused ion beam microscopy

Fengzai Tang , Yiqing Chen & Liangchi Zhang

To cite this article: Fengzai Tang , Yiqing Chen & Liangchi Zhang (2012) Analysis of polished polycrystalline diamond using dual beam focused ion beam microscopy, Philosophical Magazine, 92:13, 1680-1690, DOI: [10.1080/14786435.2012.657706](https://doi.org/10.1080/14786435.2012.657706)

To link to this article: <http://dx.doi.org/10.1080/14786435.2012.657706>



Published online: 07 Feb 2012.



Submit your article to this journal [↗](#)



Article views: 150



View related articles [↗](#)



Citing articles: 5 View citing articles [↗](#)

## **Analysis of polished polycrystalline diamond using dual beam focused ion beam microscopy**

Fengzai Tang, Yiqing Chen and Liangchi Zhang\*

*School of Mechanical and Manufacturing Engineering,  
The University of New South Wales, NSW 2052, Australia*

*(Received 12 July 2011; final version received 23 December 2011)*

This paper presents a study on polycrystalline diamond (PCD) polished by dynamic friction polishing (DFP) with the aid of advanced dual beam FIB (focused ion beam) microscopy. After disclosing a variety of wear tracks by DFP using electron imaging in combination with the ion channelling effect, a dual beam FIB was successfully employed at wear track sites to specifically create both the large cross-sectional specimen for microanalysis and thin foil for nanoanalysis. The study concluded that the polished PCD subsurface was free from microscale cracking. However, the attached debris layer on the top surface contained metal oxides and non-diamond carbon phase with inhomogeneous distributions of C, Fe, Cr, Ni, Si and O across the layer. An attached layer directly above a diamond grain was composed of essentially amorphous carbon, suggesting that a direct phase transformation from diamond crystalline to amorphous occurred during DFP.

**Keywords:** diamond; microstructure; nanostructures; focused ion beam; SEM; HRTEM; EELS; EDS

### **1. Introduction**

Polycrystalline diamond (PCD), either sintered at high temperatures and pressures [1] or fabricated by a chemical vapour deposition [2], has wide applications in, for example, cutting tools and thermal management. Traditionally, diamond crystal can be polished by pressing it against a rotating cast-iron wheel (a so-called ‘scaife’) charged with abrasive diamond grits, or a diamond bonded wheel [3]. This method can be modified by either adding oxidative agents [4] or employing high temperature [5] to improve material removal rate or surface finish. Abrasive polishing of diamond involves two- and/or three-body abrasive wear processes, and is known as anisotropy with ‘soft’ and ‘hard’ directions [6]. A recent simulation model by Pastewka et al. in 2011 [7] proposed that an amorphous layer was able to be initiated from diamond crystal by mechanically steered dissociation of individual crystal bonds during polishing. Dynamic friction polishing (DFP), as an abrasive-free technique, has been proven to be effective and efficient in polishing both single crystal [8–10] and polycrystalline diamond [11–13], where a metal disk is applied as a

---

\*Corresponding author. Email: liangchi.zhang@unsw.edu.au

counterpart similar to abrasive polishing. Contrary to the early ‘micro-cleavage’ mechanism [3], carbon phases different from diamond have been identified in ejected debris produced by both mechanical polishing [14,15] and DFP [12,13]. However, such examinations could not determine whether or not non-diamond carbon phases originated from the surface of the polished diamond grains or were formed later, after being detached from the polished sites. Hence, the underlying mechanism of diamond polishing has not reached a consensus.

High resolution transmission electron microscopy (HRTEM) in association with electron energy loss spectrum (EELS) analysis has the capabilities of resolving the atomic structure and different carbon phases [13–15], but its application is constrained for diamond materials due to shortcomings in conventional specimen preparation, which are time-demanding and non-site selective [16]. Dual beam FIB (focused ion beam) microscopy, i.e. a FIB incorporated into a scanning electron microscope (SEM), has been widely applied for TEM specimen preparation, for example, *in situ* and *ex situ* methods in materials science and geosciences [16–19]. The principle of FIB is analogous to SEM, where Ga ions are accelerated and focused on the surface of a sample. The interaction between impinging Ga<sup>+</sup> ions and the target solids can generate secondary electrons and also cause some surface atoms to be ejected as secondary ions [20]. This ion-induced secondary electron (SE) image is well-known to reflect crystallographic contrast in metals due to an ion channelling effect [20,21], while the ‘sputtering’ of target atoms can be used to site-specifically process specimen for microanalysis.

In an attempt to better understand the material removal mechanism of PCD during DFP, this paper will extend the dual beam FIB channelling effect and site-specific specimen preparation technique for the study of polished PCD. This will enable direct surface imaging of wear tracks combined with the ion channelling effect, and allow precise cross-sectioning of a polished surface for both SEM and TEM investigations into the micro- and nano-structure and phase transformation.

## 2. Experimental

The specimens used for DFP were thermally stable polycrystalline diamonds (PCD) sintered at high temperatures and pressures with silicon/silicon carbide as binder phases. Two types of PCD were studied, as shown in Table 1: one (#1) contained over 95% diamonds with an initial surface roughness of 4 μm Ra (Ringwood

Table 1. Summary of polished PCD samples.

Sample	#1	#2A	#2B
Constitution of diamond (wt%)	>95%	75	75
Nominal grain size of diamond	Varied	25	25
Polishing speed (m/s)	30	20	25
Pressure (MPa)	5	2.7	2.7
Polishing time (min)	3	3	3
Removal of debris layer	Yes	No	Yes

Diamond Material Technologies Pty. Ltd.), while the other (#2) contained about 75% polycrystalline diamond particles with an initial surface roughness of 1.7  $\mu\text{m Ra}$  (Supreme SuperHard Materials Corp.). The specimen was about 12.7 mm in diameter and 4 mm in thickness, weighting approximately 1.7 g. The dynamic friction polishing (DFP) experiment, as detailed in [11–13], was conducted by pressing a rotating PCD specimen at a designated pressure onto a rotating metal disk containing Fe, Cr, Ni and Mn in a dry atmosphere. To achieve a better polishing performance, the PCD specimen also rotated. The polishing conditions are listed in Table 1. The surface roughness of the specimen was reduced from its initial range of 1–4  $\mu\text{m Ra}$  to 0.1–0.5  $\mu\text{m Ra}$  after polishing. The attached debris layer on the surface of the polished PCD (specimen #1 and #2B) was removed by a mixed acid solution of HCl and  $\text{HNO}_3$ .

### **2.1. Surface morphology of the polished PCD**

The surface morphology of on Sample #1 was first examined using a dual beam FIB with a high resolution field emission SEM (FEI Nova NanoLab<sup>TM</sup>). Two imaging modes were employed in acquiring the secondary electron (SE) micrographs, i.e. electron beam-induced and  $\text{Ga}^+$  ion beam-induced SE images [20], using an Everhart–Thornley detector.

### **2.2. Cross-sectional specimen prepared by FIB for microanalysis**

To examine the microstructure of the PCD underneath the polished surface and that of the attached debris layer, a specimen was mechanically separated from Sample #2A with the attached debris layer on top of the polished surface. Subsequently, a large cross-sectional region was milled by FIB (FEI NanoLab<sup>TM</sup>). The phase information in the PCD matrix and cross-sectional attached layer was examined using a Raman (Renishaw inVia)/SEM (FEI Quanta<sup>TM</sup> 200 3D) for a combined structural chemical analysis, where an argon laser (541.5 nm) was used to excited the specimen at a power of 10 mW. The chemical composition of the specimens was also examined using a high resolution SEM (Zeiss ULTRA plus) fitted with an energy dispersive X-ray spectrometer (EDS), where line scans and elemental mapping were performed to reveal the microstructures.

### **2.3. Cross-sectional specimen prepared by FIB for TEM analysis**

A TEM foil was prepared using *in situ* lift-out method on Sample #2B [18,19], where the majority of the debris layer on its surface was removed by a mixed acid solution followed by light mechanically cleaning. A thin Au layer was coated to protect the polished interface from Ga damage, before a Pt strap was deposited on the surface inside the FIB microscope. The FEI NanoLab<sup>TM</sup> microscope was employed for cutting and final milling because there was no micromanipulator inside the microscope. The FEI Quanta<sup>TM</sup> microscope was used for *in situ* lifting where a micromanipulator (Kleindiek) was fixed inside the chamber. The obtained TEM foil

was examined using a high resolution TEM (JEOL 3000 F–300 kV) with both EDS and EELS.

### 3. Results

#### 3.1. Surface morphology of polished PCD and ion channelling

The polished PCD surface of Sample #1 was thoroughly examined, as depicted in Figure 1. Figure 1b and e are ion-induced SE images; the others are electron-induced SE images. The specimen surface in Figure 1a was placed horizontally, but the surface was tilted to  $52^\circ$  in all other images. Tiling the specimen surface can enhance the surface topography for electron-induced SE imaging but, with the exception of Figure 1c with an Au-coated surface, all the others were directly imaged. It should be noted that Figure 1d–f were taken from a specimen whose surface was slightly cleaned using alumina paper after acid-soaking.

Although more fine structures can be identified from a specimen surface using electron beam excitation, it is clear that ion beam-induced SE imaging (Figure 1b) presents an excellent contrast for demonstrating each individual grain due to the ion channelling effect [20,21]. This is because when the normal of a crystal plane is aligned with the direction of the ion beam, ions may penetrate deeper through collision cascade in a relative lower index direction, in which a lower yield of secondary electron will be generated resulting in a relative darker area in the SE image. Thus, the contrast of the image varied with the crystallographic orientations of individual grains in the PCD specimen. From Figure 1b, a wide range of diamond grain dimensions with irregular shapes is easily discernible, ranging from submicron

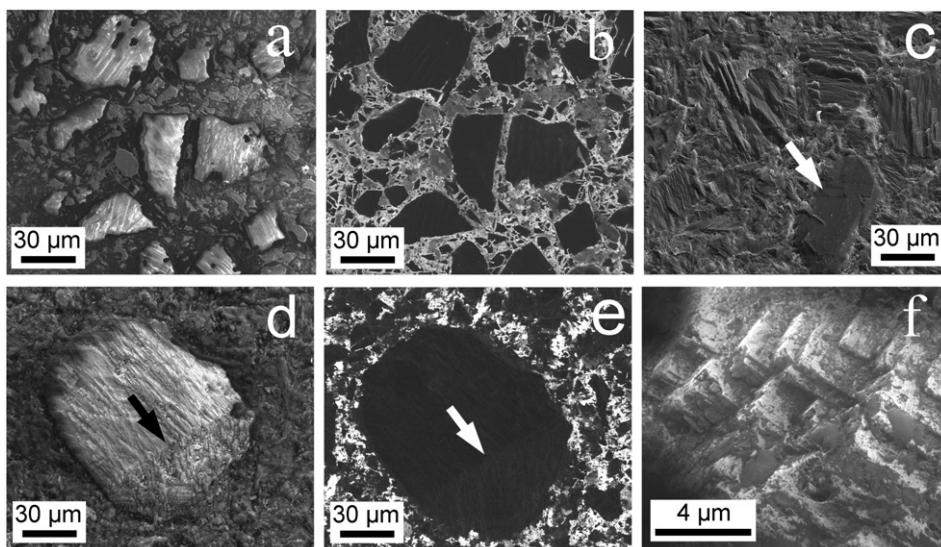


Figure 1. Surface morphology of polished PCD specimen #1. (b, e) Ion-induced SE images. (a, d, c, f) Electron-induced SE images. (c) Image from an Au-coated surface; all others are imaged directly from the specimen surface without coating. Details in text.

to a few tens of microns. Some of them have sharp edges, showing the characteristics of the crystal.

Figure 1a and c present a variety of wear tracks, in which some bands of 'grooves' are aligned in specific directions in the grains. An examination shows that the spacing of the 'groove' bands range from a submicron scale to a few microns. Some large diamond grains also depict relative 'flat' surfaces up to a few tens of microns, as shown in Figure 1c marked by an arrow. Interestingly, two distinct wear tracks appear on a single diamond grain (Figure 1d and e). The different directions of the wear tracks from the interface, as indicated by the arrow in the electron beam-induced image in Figure 1d, can be clearly discerned. The corresponding ion beam-induced image in Figure 1e shows slightly different contrasts on two wear areas. In addition, a set of crystal planes with 'sharp edges' on a microscale was also coincidentally disclosed from the grain shown in Figure 1f. It is assumed that the apparent disbondment between the grains and the matrix in the electron-induced images (Figure 1a and d) was mainly caused by the charging effect at the interface while acquiring the images. Such feature cannot be consistently observed in the ion-induced images (Figure 1b and e) and in the image from the Au-coated specimen (Figure 1c). Hence, although the disbondment between the grains and matrix may occur at the polished surfaces, it is not significant.

It was also found that the channelling effect degraded rapidly with extended exposure of the ion beam. For instance, exposure on a defined area of  $400 \times 400 \mu\text{m}$  for about 1 min at 30 kV and 3 nA led to complete loss of contrast. Therefore, a low ion beam current of 10–30 pA at 30 kV was employed while acquiring ion-induced SE images. The ion channelling effect was not perceived in the Au-coated sample.

### 3.2. Microanalysis of cross-sectional polished PCD

A large cross-section of polished surface was milled by FIB from PCD #2A with an attached debris layer. Figure 2a is a SE image of a freshly made specimen (tilted  $52^\circ$ ), which clearly depicts the microstructure underneath the polished surface. Some grains appeared with crystalline feature of sharp edges. In general, the debris layer has a wide range of thickness depending on the specific surface topography of hard matrix. The apparent cracks between the hard matrix and the attached layer could have resulted from specimen preparation of mechanical breaking, but the white interface, as indicated by the white arrow, remained unclear before EDS mapping was conducted.

As regards Raman/SEM analysis, fine mapping of the phase distributions across the adhesive layer was unresolved due to the large beam size and a lack of stage automation between Raman and SEM. The coarse-spaced analysis is circled in Figure 2a. The Raman spectrum of natural diamond displayed a single sharp peak at  $1332 \text{ cm}^{-1}$  [22] and thus the peak ( $1332 \text{ cm}^{-1}$ ) identified in Spectrum *i* in Figure 2b can be assigned to  $\text{sp}^3$ -bonded diamond. The close matching implies a negligible stress effect [23]. From the analysis of the debris layer at location *ii*, both a non-diamond carbon phase and metal oxides were observed. Previous studies [23–25] have reported that graphitic  $\text{sp}^2$ -bond carbon has two first-order peaks at  $1357 \text{ cm}^{-1}$  (D band) and  $1580 \text{ cm}^{-1}$  (G band), while disordered and non-crystalline graphitic

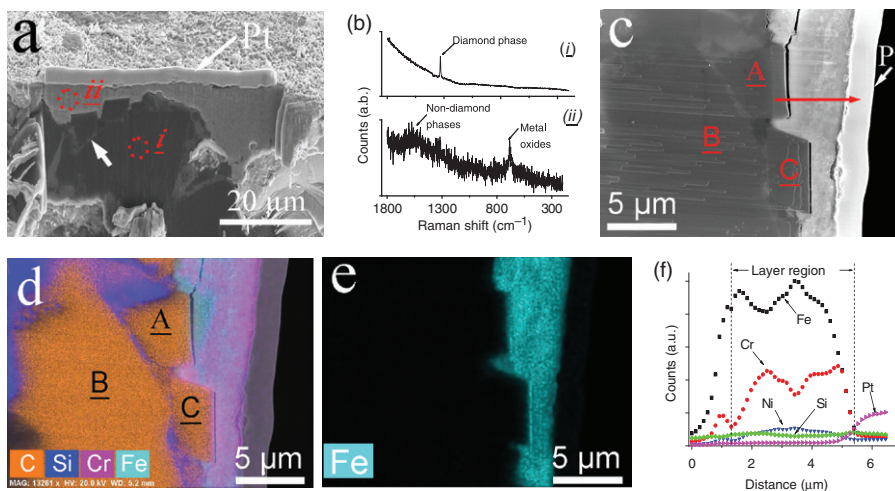


Figure 2. Microanalysis of polished PCD #2A. (a) A freshly FIB processed cross-sectional specimen, where the marked positions *i* and *ii* are for Raman/SEM analysis in (b). (b) Raman analysis result. (c) SE image of part of (a) for EDS mapping, with the line showing the position of the line-scan in (f). (d) EDS mapping of C (yellow), Si (blue), Cr (pink) and Fe (cyan) superimposed on a SE image of (c). (e) Fe (cyan) mapping for clarity only. (f) EDS line-scan across the attached layer. (d, e) Colour on-line.

carbon, amorphous diamond-like-carbon and glass carbon have a pair of broad D and G bands with shifting positions and a varied intensity ratio of D/G. Thus, the non-diamond carbon band centred at  $\sim 1570\text{ cm}^{-1}$  in Spectrum *ii* of Figure 2b tends to be a more highly disordered  $\text{sp}^2$  hybrid carbon. Since iron oxides and chromium oxides could generate a Raman shift at  $676$  and  $618\text{ cm}^{-1}$ , respectively [26], the peak centred at  $\sim 680\text{ cm}^{-1}$  could have stemmed from metal oxides as the peak could be shifted due to its local environment. These metal elements, such as Fe, Cr and Ni, in the debris layer were generated by the polishing disk sliding in contact with the sample surface during DFP. This is consistent with the following EDS analysis and previous investigations on the top surface and ejected debris [12,24].

Part of the cross-sectional image of Figure 2a was selected for EDS analysis, as depicted in Figure 2c. Figure 2d is the corresponding elemental mappings of C (yellow), Si (blue), Cr (pink) and Fe (cyan) superimposed on the SE image, while Figure 2e, for Fe (Cyan), is for comparison only. For each mapped element, different filtering thresholds were employed for clarity. From elemental mapping, the white interface, as depicted by the white arrow in Figure 2a, is clearly Si-rich, which consolidates the idea that it was neither re-deposited contaminants during FIB processing nor artificial cracks caused by specimen breaking. For convenience of discussion, we have labelled the three large diamond grains as ‘A’, ‘B’ and ‘C’ in Figure 2c and d, where the boundaries of these grains can be easily distinguished due to the present of silicon (in blue) in Figure 2d. Another cross-sectional specimen from a polished PCD of  $\sim 6$  microns in size was also examined and no microscale cracks were observed (data not shown).

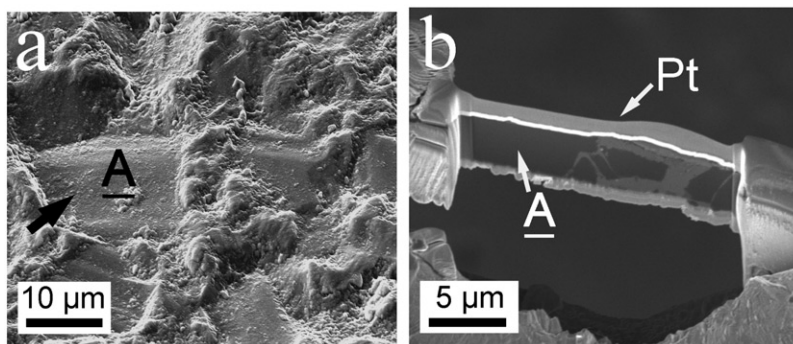


Figure 3. SE images of (a) a chosen diamond grain of 'A' for *in situ* lift-out TEM foil preparation (PCD #2B). (b) An almost finished TEM specimen mounted on a Cu grid, which reveals a few diamond grains as dark areas.

In Figure 2c, a sharp edge of Grain 'C' was inclined against the normal of its top surface, and the height difference between Grains 'A' and 'C' is about 1.5  $\mu\text{m}$ . From a few line-scans, a number of elements, C, O, Fe, Cr, Ni and Si, were found with uneven distributions across the attached debris layer. Although the profile appeared to be site-dependent; in general, the carbon count was very low and less than that of oxygen. One of the line-scans is shown in Figure 2f, whose position is delineated in Figure 2c ( $\sim 4\text{ mm}$  thick). In this figure, the profiles of Fe, Cr, Ni and Si are selected for clarity, and the Pt profile acts as a boundary reference. Since the interaction volume between the microprobe and target specimen in EDS analysis may be greater than 1  $\mu\text{m}$ , it results in a 'tail-off' on both sides of the profile.

### 3.3. Nanoanalysis of cross-sectional polished PCD #2B

To prepare a cross-section specimen for TEM analysis, a diamond grain with a relative flat surface was chosen for *in situ* lift-out, marked as 'A' in Figure 3a, where the sample surface was tilted  $52^\circ$ . Figure 3b presents an almost completed TEM specimen, which was taken from bulk PCD compact and mounted on a Cu grid (Omniprobe<sup>TM</sup>). From the figure, a few diamond grains are clearly identified as dark areas and again there is no noticeable microscale crack. The bright curve underneath the Pt strap is the pre-coated Au layer, which clearly illustrates the evolution of the polished PCD surface. The relatively straight Au line above grain 'A' indicates that the exposed surface was flat with a submicron scale after polishing. A TEM specimen prepared in this manner can be returned to the FIB microscope for further thinning until it is sufficiently thin for TEM analysis.

The nanostructure of the polished PCD interface was examined using a HRTEM. Figure 4 depicts part of the cross-sectional view of a polished diamond grain (Grain 'A' in Figure 3a). In Figure 4a, a debris layer of varied thickness along the surface of the grain is revealed between the top surface of the diamond and the coated Au layer, where a diffraction pattern with a  $\langle 011 \rangle$  zone axis from the diamond grain is also superimposed (The rotation between image and diffraction

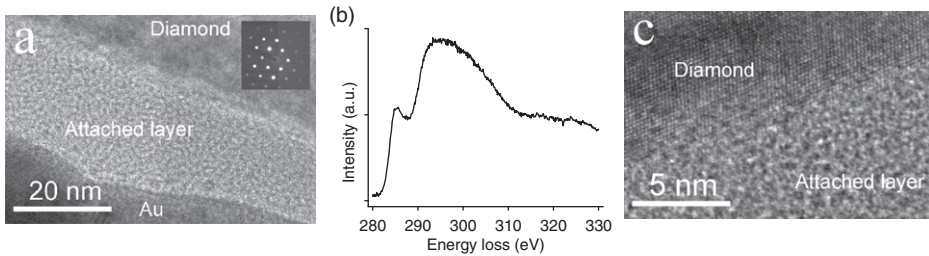


Figure 4. TEM analysis of polished PCD #2B. (a) View of the attached layer on the top of a diamond grain (grain ‘A’ in Figure 3a) and an insert diffraction pattern of a diamond grain with a  $\langle 011 \rangle$  zone axis. (b) High-loss EELS of the attached layer, where the carbon K edge is set at 285 eV. (c) High magnification image of the interface between the diamond grain and attached layer.

pattern was not calibrated in this case). The lattice fringes can be easily observed for both diamond and Au layer at the higher magnification. The evolution of the interface between the diamond grain and the attached layer shows that, in this case, the polished surface is not flat with a nanometre scale. The investigation by nanobeam diffraction and EDS analysis indicates that the attached layer is essentially amorphous carbon, which is consistent with EELS analysis (Figure 4b). This high-loss spectrum can be assigned to amorphous carbon, where the first pre-edge peak positioned at 285 eV may account for the transition from an inner shell  $1s$  to  $\pi^*$  states of carbon atoms [13–15]. Figure 4c is a high magnification image taken at the interface between the diamond and attached layer, in which the atomic lattice of the diamond grain is clearly visible, in contrast to the amorphous nature of the attached layer. Since atomic lattices in the upper protective Au layer were clearly observed at high magnification, the identified amorphous carbon layer in this case could not be an artefact due to the amorphorisation of the diamond surface upon Ga implantation.

## 4. Discussion

### 4.1. Origin of the wear tracks

Surface examination of the polished PCD shows diverse wear tracks (Figure 1), featured as ‘grooves’ with different scales and ‘plate-like surfaces’ up to the micron scale. A band of ‘grooves’ in an individual grain appears with a high degree of regularity in terms of their orientation and inter-spacing. However, such orientation and inter-spacing vary from one grain to another. This suggests that polishing had a function of orientation selection for a particular plane of a diamond grain, and the grain could be polished only when it was aligned in a ‘soft’ direction. It is possible that the generation of ‘grooves’ on the surface of the diamond grain was caused by the different material removal rates along different crystallographic orientations.

It is well known that a single crystalline diamond exhibits anisotropic features under mechanical polishing. There are ‘soft directions’, which have higher material removal rates on specific planes, such as the  $\langle 100 \rangle$  direction on the  $\{100\}$  and  $\{110\}$  planes. There are also ‘hard directions’ which have lower material removal rates,

such as the  $\langle 110 \rangle$  direction on the  $\{100\}$  and  $\{110\}$  planes and all directions on the  $\{111\}$  surface [3,7]. The feature of the 'grooves' has also been disclosed in different scales during abrasive polishing of single crystalline diamond [6,27,28]. Hird et al. [28] proposed that small diamond particles generated from the fracture of the diamond grain during polishing, instead of the asperity of replenished diamond abrasives, may be responsible for the 'nano-grooving' on the polished diamond surface. PCD consists of individual diamond crystallites bonded together in random crystallographic orientations. It is reasonable to assume that such a mechanism might also contribute to the generation of the 'grooves' in DFP, as found in this work. During DFP processing, both the PCD specimen and the polishing disk rotate. Therefore, the diamond material was possibly polished selectively along a relatively soft direction on a given plane of a grain.

#### **4.2. Polishing mechanism of PCD with respect to observed evidences**

Considering the friction-induced high temperature in DFP [8–10], the polishing mechanism could be related to a number of factors, such as thermal, chemical, normal and shear stressing. This can be seen from the large diverse wear tracks in the polished PCD surface (Figure 1). The 'grooves' in the wear tracks imply 'plastic deformation', and phase transformation of the diamond to non-diamond could occur during polishing. However, the 'sharp edges' feature in Figure 1f may be a result of occasional 'micro-chipping'. Thus, it is rational to assume that removing material from diamond during polishing could be a result of multiple mechanisms, and could be site- (or grain-) dependent in different sequences subject to the crystallographic orientation of a grain and localised polishing conditions.

Raman/SEM and EDS microanalysis on the debris layer in Figure 2 shows the formation of metal oxides (i.e. iron oxides and chromium oxides) and a non-diamond carbon phase. This is consistent with previous analyses on ejected debris [10,12,13]. The observation of a non-diamond carbon phase is also in line with site-specific TEM analysis, where amorphous carbon was identified in the attached layer on the top of a diamond grain. This suggests that a direct phase transformation from hybrid  $sp^3$  diamond to  $sp^2$  carbon occurred during the polishing process. At atmospheric pressure, diamond is an unstable form of carbon, whereas it can convert to graphite in appreciable rates only at high temperatures over  $1700^\circ\text{C}$  [29]. It is also known that diamond had a strong affinity for transitional metals, and a chemical reaction occurs at relatively low temperatures, e.g. at  $800^\circ\text{C}$ , in contact with iron plate in a vacuum without sliding motion [30]. In DFP, the interface flash temperature between the PCD and metal plate can be estimated at over  $1000^\circ\text{C}$  due to frictional heating [9,11], where transitional metals may act as a catalyst for a thermochemical reaction. Thus, diamond could degrade its lattice structure and be converted into non-diamond carbon phases, presumably including both amorphous and other noncubic diamond polytypes (e.g. graphitic carbon), after which the material can be easily removed. It is thought that this conversion is different from abrasive polishing, where material removal is proposed via mechanically steered dissolution of the diamond structure [7].

## 5. Conclusions

The microstructure of polished PCD produced by dynamic friction polishing has been studied from the micrometre level to a nanometre scale using an advanced dual beam FIB technique. The following conclusions can be drawn:

- A remarkable ion channelling effect was observed in a polished PCD surface (non-coated specimen), from which the size distribution of the diamond grain was revealed. Examination of the polished surface showed a variety of wear tracks, with prominent 'groove' band and a microscale 'plate-like surface'.
- From large cross-sectional PCD specimens, microscale cracks were not found beneath the polished PCD surface, although a specimen was found to have a large surface height difference between two adjacent diamond grains. Non-diamond carbon phase and metal oxides were identified in the debris layer, in which inhomogeneous distributions were found for a range of identified elements (Fe, Cr, Ni, Si, O and C).
- An *in situ* lift-out method was successfully developed to prepare a TEM specimen which was thin enough for high resolution imaging of the atomic lattice of diamond and also for EELS analysis.
- The variety of wear tracks indicated the complexity of the material removal mechanism in DFP, including plastic deformation and occasional cleavage. The observation of amorphous carbon from the material remaining directly on the surface of a polished diamond grain suggested that an allotropic transformation of diamond crystal to amorphous could take place during polishing. This is consistent with the observation of a non-diamond phase by Raman/SEM analysis in the debris layer.

## Acknowledgements

The authors thank the staff of AMMRF, Charlie Kong of the University of New South Wales (UNSW) for his help in specimen preparation and Shaun Bulcock of the University of Sydney (USyd) for training in EELS analysis. Peter Felfer at USyd and Leonard Green of the University of Adelaide are also acknowledged for their help. This work was funded by Australian Research Council.

## References

- [1] A.E. Ringwood, Diamond compact possessing low electrical resistivity, US Patent 5106393, 1992.
- [2] J.J. Gracio, Q.H. Fan and J.C. Madaleno, *J. Phys. D: Appl. Phys.* 43 (2010), Article No. 374017.
- [3] E.M. Wilks and J. Wilks, *J. Phys. D: Appl. Phys.* 5 (1972) p.1902.
- [4] C.Y. Cheng, H.Y. Tsai, C.H. Wu, P.Y. Liu, C.H. Hsieh and Y.Y. Chang, *Diamond Relat. Mater.* 14 (2005) p.622.
- [5] N. Furushiro, M. Higuchi, T. Yamaguchi, S. Shimada and K. Obata, *Precision Eng.* 33 (2009) p.486.
- [6] J.R. Hird and J.E. Field, *Proc. R. Soc. Lond. A* 460 (2004) p.3547.

- [7] L. Pastewka, S. Moser, P. Gumbsch and M. Moseler, *Nat. Mater.* 10 (2011) p.34.
- [8] K. Suzuki, N. Yasunaga, Y. Seki, A. Ide, N. Watanabe and T. Uematsu, *Proc. ASPE* 14 (1996) p.482.
- [9] M. Iwai, T. Uematsu, K. Suzuki and N. Yasunaga, *Proc. ISAAT IV* (2001) p.231.
- [10] K. Suzuki, M. Iwai, T. Uematsu and N. Yasunaga, *Key Eng. Mater.* 238–239 (2003) p.235.
- [11] Y. Chen, L.C. Zhang, J.A. Arsecularatne and C. Montross, *Int. J. Mach. Tool Manuf.* 46 (2006) p.580.
- [12] Y. Chen, L.C. Zhang and J.A. Arsecularatne, *Int. J. Mach. Tool Manuf.* 47 (2007) p.1615.
- [13] Y. Chen, L.C. Zhang, J.A. Arsecularatne and I. Zarudi, *Int. J. Mach. Tool. Manuf.* 47 (2007) p.2282.
- [14] S.E. Grillo and J.E. Field, *J. Phys. D: Appl. Phys.* 30 (1997) p.202.
- [15] F.M. van Bouwelen, J.E. Field and L.M. Brown, *Philos. Mag.* 83 (2003) p.839.
- [16] L.F. Dobrzynetska, H.W. Green, M. Weschler, M. Darus, Y.C. Wang, H.J. Massonne and B. Stockhert, *Earth Planet. Sci. Lett.* 173 (2003) p.399.
- [17] F. Tang, B. Gault, S.P. Ringer and J.M. Cairney, *Ultramicroscopy* 110 (2010) p.836.
- [18] P.R. Munroe, *Mater. Charact.* 60 (2009) p.2.
- [19] R. Wirth, *Chem. Geol.* 261 (2009) p.217.
- [20] R. Levi-setti, T.R. Fox and K. Lam, *Nucl. Instrum. Methods* 205 (1983) p.299.
- [21] R.E. Franklin, E.C.G. Kirk, J.R.A. Cleaver and H. Ahmed, *J. Mater. Sci. Lett.* 7 (1988) p.39.
- [22] S. Praver and R.J. Nemanich, *Phil. Trans. R. Soc. A* 362 (2004) p.2537.
- [23] C. Johnston, A. Crossley, P.R. Chalker and J.M. Buckley-Golder, *Diamond Relat. Mater.* 1 (1992) p.450.
- [24] J.R. Hird, M. Bloomfield and I.P. Hayward, *Philos. Mag.* 87 (2007) p.267.
- [25] D.S. Knight and W.B. White, *J. Mater. Res.* 4 (1989) p.385.
- [26] S.C. Tjong, *Mater. Res. Bull.* 18 (1983) p.157.
- [27] M.S. Couto and W.J.P. van Enckevort, *Philos. Mag. B* 69 (1994) p.621.
- [28] J.R. Hird, M. Bloomfield and I.P. Hayward, *Philos. Mag.* 87 (2007) p.267.
- [29] Y.G. Gogotsi, A. Kailer and K.G. Nickel, *J. Appl. Phys.* 84 (1998) p.1299.
- [30] H. Tokura, C.F. Yang and M. Yoshikawa, *Thin Solid Films* 212 (1992) p.49.